Quantum fuel with multilevel atomic coherence for ultrahigh specific work in a photonic Carnot engine

Deniz Türkpençe* and Özgür E. Müstecaplıoğlu
Department of Physics, Koç University, İstanbul, Sarıyer 34450, Turkey
(Received 8 October 2015; published 27 January 2016)

We investigate scaling of work and efficiency of a photonic Carnot engine with a number of quantum coherent resources. Specifically, we consider a generalization of the "phaseonium fuel" for the photonic Carnot engine, which was first introduced as a three-level atom with two lower states in a quantum coherent superposition by M. O. Scully, M. Suhail Zubairy, G. S. Agarwal, and H. Walther [Science **299**, 862 (2003)], to the case of $N+1$ level atoms with N coherent lower levels. We take into account atomic relaxation and dephasing as well as the cavity loss and derive a coarse-grained master equation to evaluate the work and efficiency analytically. Analytical results are verified by microscopic numerical examination of the thermalization dynamics. We find that efficiency and work scale quadratically with the number of quantum coherent levels. Quantum coherence boost to the specific energy (work output per unit mass of the resource) is a profound fundamental difference of quantum fuel from classical resources. We consider typical modern resonator set ups and conclude that multilevel phaseonium fuel can be utilized to overcome the decoherence in available systems. Preparation of the atomic coherences and the associated cost of coherence are analyzed and the engine operation within the bounds of the second law is verified. Our results bring the photonic Carnot engines much closer to the capabilities of current resonator technologies.

DOI: 10.1103/PhysRevE.93.012145

I. INTRODUCTION

A practical figure of merit to compare fuel and battery materials is the specific energy or energy-to-mass ratio [1–3]. As a material constant, it measures the energy that will be harvested by using a unit mass of the material. About a decade ago, a highly nontraditional fuel, called "phaseonium," which is a three-level atom with two lower states in a quantum coherent superposition, was proposed to be used in a photonic Carnot engine (PCE) [4]. A phaseonium engine could work with a single heat bath and a phaseonium reservoir [4–7]. This proposal stimulated much interest to quantum heat engines [8–20]. It was later argued that existing resonator systems cannot implement such an engine, due to high cavity losses and atomic dephasing [21]. Here we address a fundamental question of how the specific energy of phaseonium fuel is scaled with the number of quantum coherent levels. A favorable scaling law against decoherence and dephasing could bring the phaseonium engine closer to available practical systems.

We describe a multilevel generalization of phaseonium fuel in Fig. 1. The block-diagonal density matrix ρ of an $N+1$ level atom is shown in Fig. 1(a). The excited level, denoted by "a," and the lower levels, denoted by "$b_1, b_2, \ldots, b_N$," are well separated from each other by an energy Ω measured from the central lower level $b_{N/2}$ as shown in Fig. 1(b). The lower levels can be degenerate or nondegenerate. The diagonal elements ρ_{aa}, and ρ_{bb}, with $b \in \{b_1, b_2, \ldots, b_N\}$, determine the level populations, while the off-diagonal elements $\rho_{bb'}$, with $b' \neq b$, indicate the coherence between the levels. Coherence can be characterized by the magnitude and phase of the complex number $\rho_{bb'}$.

Though both the amplitude and the phase of coherent superposition states can be controlled in experiments [22], the main control variable for the photonic Carnot engine is the phase of the coherence as the amplitude is required to be small enough to keep the system only slightly out of thermal equilibrium. The complete graphs in Fig. 1(a) have N nodes and $N(N-1)/2$ links, representing the atomic energy levels and the coherences between them, respectively. The simplest graph has $N=2$ nodes, which is the case of the original phaseonium proposal [4]. The interplay between quantum coherence and energy discussed in the photon Carnot engine [4] revealed that the energy content of the phaseonium with $N=2$ can be optimized at a certain phase of the coherence. We could envision as if we are considering more complex, larger, phaseonium molecules with the graphs having $N>2$, corresponding to $N+1$ level atom phaseonium (NLAP).

We can imagine different phaseonium molecules can be possible for a given atom of unit mass and explore how the specific energy of the atom depends on the size of the phaseonium molecule characterized by N. Next to the phase of coherence, N becomes another control parameter which could favorably contribute to the enhancement of the specific energy of the single-atom quantum fuel. For $N \gg 1$, the number of coherences would scale quadratically, $\sim N^2$. If the quadratic coherence scaling could be translated into the energy content of the atomic fuel, then we could overcome the cavity losses for implementation and boost the performance of quantum Carnot engine for applications. From a fundamental point of view, such a scaling analysis could reveal a profound difference of quantum fuel from a classical resource, as such a scaling cannot exist without quantum coherence. Complete graphs of phaseonium molecules serve as more than a simple counting of coherences. They emphasize the generality of our question we address in the present contribution. Can we beat decoherence with the scaling advantage of quantum coherent resources?

*dturkpence@ku.edu.tr

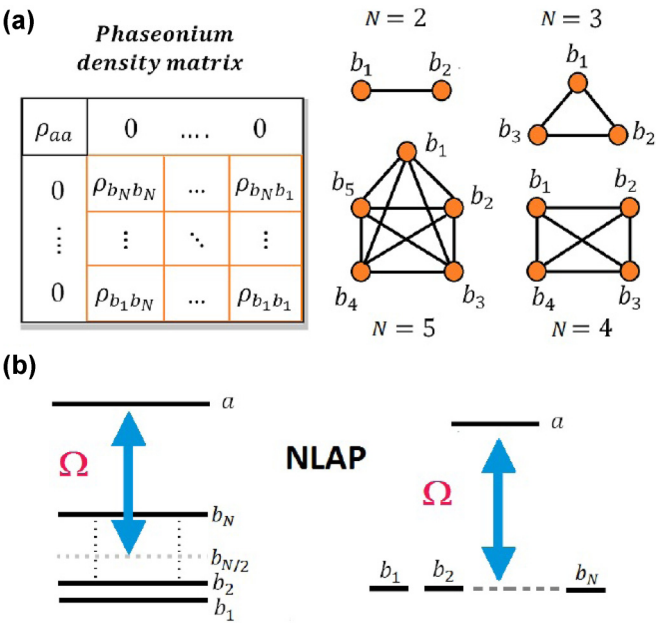

FIG. 1. $N+1$ level atom phaseonium (NLAP) fuel. (a) Density matrix ρ and complete graph representations of NLAP. ρ is $N+1$ dimensional square matrix. Its coherent block can be represented by a complete graph with N nodes and $S = N(N-1)/2$ links. Graphs were shown up to $N = 5$ number of nodes. (b) NLAP for nondegenerate and degenerate atoms. The excited state is denoted by a and the lower levels are denoted by b_i with $i = 1, \ldots, N$. The upper level is well separated from the lower levels by an energy $\hbar\Omega$ measured from the central lower level $b_{N/2}$.

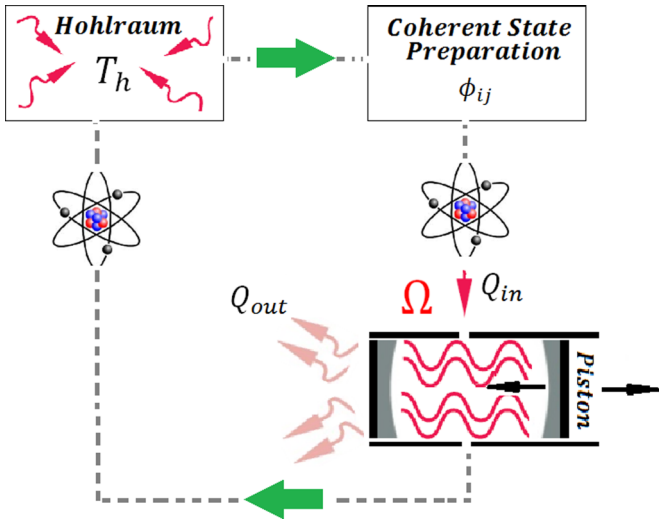

FIG. 2. Photonic Carnot engine with $N+1$-level atom phaseonium (NLAP) fuel. Photon gas in a high-quality cavity of frequency Ω is the working substance and the mirrors of the cavity play the role of the piston. NLAP leaves the hohlraum at temperature T_h and is subsequently prepared in a state with quantum coherence among its lower levels characterized by $N(N-1)/2$ phase parameters ϕ_{ij} with $i, j = 1, \ldots, N$. Created NLAPs are repeatedly injected into the cavity at a rate r in the quantum isothermal expansion process, where heat Q_{in} is transferred to the cavity. The cycle continues with quantum adiabatic expansion and quantum isothermal compression and is completed with a quantum adiabatic compression. An amount of heat Q_{out} is rejected into the entropy sink in the isothermal compression.

We have recently proposed a superradiant quantum Otto engine [20] where clusters of N two-level atoms prepared in thermal coherent spin states are used as a quantum fuel. This engine is also capable to exhibit a similar quadratic scaling law of work with N; however, the efficiency is independent of the temperature and N. Superradiant engine has no analytical master equation and numerical analysis reveals that the quantum coherence serves as a catalyst, increasing the energy injection rate into the photonic working medium from the atomic clusters. In the case of a photonic Carnot engine with N-level phaseonium fuel, an analytical master equation reveals that the quantum coherence serves effectively as a resource. In superradiant Otto engine, two heat baths are considered; while photonic Carnot engine is used to explore harvesting work from a single heat bath. Moreover, Carnot efficiency depends on the temperature and exhibits quadratic scaling with the number of levels N. Furthermore, even though the work output scales quadratically with N for both engines, specific energy of coherent cluster fuel increases linearly with the number of atoms N; while it has quadratic scaling with the number of coherent levels N of the phaseonium fuel. The linear increase of the mass of the unit atomic cluster with the number of atoms degrades the quantum coherent advantage in the specific energy. A quantum advantage in the charging power of quantum batteries with the number of qubits has been examined very recently [23]. Linear scaling of work with the number of qubits is reported, whereas, due to a quantum speed up of the operation time, the charging power scales quadratically [23]. The preparation of phaseonium fuel and using it in PCE can be compared to charging and discharging a single qubit quantum battery with multiple quantum coherences. Phaseonium fuel or battery allows for quadratic scaling in harvested work, efficiency, and the specific energy with the number of quantum coherences. We examined the charging or preparation cost of the phaseonium battery and compared it with the harvested work by PCE. Our result verified that the second law is obeyed in our system.

This manuscript is organized as follows: In Sec. II, we describe the N-level phaseonium model and PCE system dynamics. We review and discuss the analytical and numerical verification of the analytical results in Sec. III. We also estimate the preparation cost of NLAP in this section. We conclude the results in Sec. IV.

II. NLAP MODEL AND SYSTEM DYNAMICS

The operation of photonic Carnot engine is described in Fig. 2. The working fluid of the engine is the photon gas in a high-quality single-mode cavity of frequency Ω. The radiation pressure by the cavity photons applies on the cavity mirrors playing the role of the piston of the engine. The quantum fuel of the engine is an NLAP. The quantum Carnot cycle consists of two quantum isothermal and two quantum adiabatic processes.

In the isothermal expansion, NLAPs are generated and injected into the cavity at a rate r. The interaction time τ between an NLAP and the cavity field is short, $\tau < 1/r$, so only one NLAP can be present in the cavity [24]. Coherences in NLAP are characterized by $N(N-1)/2$ phase parameters ϕ_{ij},

with $i,j = 1,2,\ldots,N$. Coherent superposition states in $N+1$ level atom system can be generated by stimulated Raman adiabatic passage (STIRAP) [25,26], Morris-Shore transformation [27], or quantum Householder reflection techniques [28,29]. Thermalization of the single atom can be considered relatively fast and hence the injection rate would be limited by the time of coherence preparation. The choice of specific technique of coherence induction depends on the details of a particular implementation. If the amplitudes of the coherences are much smaller than the level populations, then NLAP can be assumed in an approximate thermal equilibrium with a thermal reservoir (hohlraum) at a temperature T_h. During the interaction, the mean number of photons, $\bar{n}$, and the cavity temperature increases; while the expansion cools down the cavity when there is no atom inside. Repeated injection of NLAPs into the cavity maintains the cavity field at a temperature T_ϕ by transferring a total amount of heat into the cavity as $Q_{\rm in}$. T_ϕ is an effective temperature defined in terms of the steady-state photon number $\bar{n}_\phi$ as $T_\phi = \hbar\Omega/k\ln(1+1/\bar{n}_\phi)$, with k as the Boltzman constant. It can be higher than T_h in the presence of coherence [4]. The cavity volume, and hence the frequency, change negligibly, $\Delta\Omega \ll \Omega$.

The cycle continues with an adiabatic expansion where the entropy remains constant and the temperature drops as the Ω changes appreciably. The following step is the isothermal compression in which heat $Q_{\rm out}$ is transferred from cavity to a cold reservoir at a temperature T_c. The cycle is completed by adiabatic compression where the temperature is raised back to T_ϕ.

The net work extracted from the cycle is $W_{\rm net} = Q_{\rm in} - Q_{\rm out}$, where $Q_{\rm in} = T_\phi(S_2 - S_1)$ and $Q_{\rm out} = T_c(S_3 - S_4)$. The mean photon number $\bar{n}_i$ and the temperature T_i at the beginning of the $i^{\rm th}$ stage determine the entropy S_i by $S_i = k\ln(\bar{n}_i+1) + \hbar\Omega\bar{n}_i/T_i$. Using $S_1 = S_4$, $S_2 = S_3$, $T_1 = T_2 = T_\phi$, and $T_3 = T_4 = T_c$, we write $W_{\rm net} = (T_\phi - T_c)(S_2 - S_1)$. The efficiency of the engine is defined as $\eta = W_{\rm net}/Q_{\rm in}$. It reduces to $\eta = 1 - T_h/T_\phi$. This coincides with the standard definition of thermodynamic efficiency in Carnot cycle and used in the original proposal of the phaseonium fuel [4–7] as well as in the arguments against its feasibility in the presence of decoherence channels [21]. In order to present results comparable to the previous works, we calculate the efficiency as defined by these studies. To avoid any misleading impressions, however, we emphasize that in practical considerations round-trip efficiency can be more relevant figure of merit. The round-trip efficiency of the engine should include the cost of the preparation of the quantum coherent atom; which would ensure the validity of the second law [7]. On the other hand, it was noted that the cost of quantum fuel can be expensive [5], but it is still appealing as it can be used to harvest work from a single heat reservoir. Our objective here is not to discuss if such PCEs can be efficient enough for certain applications but to examine if such devices, proposed in Ref. [4], can produce positive work in the presence of decoherence by exploiting a scaling advantage of multiple coherence resources, in contrast to the negative conclusions of earlier studies [21].

During the adiabatic process $\bar{n}$ does not change so $\bar{n}_1 = \bar{n}_4 = [\exp(\hbar\Omega/kT_c) - 1]^{-1}$ and $\bar{n}_2 = \bar{n}_\phi$. These relations reveal that work and efficiency of the photonic Carnot engine can be calculated by determining the $\bar{n}_\phi$ at the end of the isothermal expansion stage.

III. RESULTS AND DISCUSSIONS

In order to find the $\bar{n}_\phi$, we solve $\dot{\bar{n}}_\phi = \sum_n n\dot{\rho}_{nn} = 0$, where $\dot{\rho}_{nn} = \langle n|\dot{\rho}|n\rangle$. Here $|n\rangle$ is the Fock number state for the cavity photons and ρ is the reduced density matrix of the cavity field. The equation of motion for ρ can be obtained by tracing the equation of motion of the complete system over atomic degrees of freedom

$$\dot{\rho}_{nn} = -\frac{i}{\hbar}\sum_k (\mathrm{Tr}_{\rm at}[H^k,\rho^k]_{nn}), \tag{1}$$

where $H^k = H_0 + H_I^k$ is the Hamiltonian of the arbitrary $k^{\rm th}$ atom in the interaction picture relative to the cavity photons, with $H_0 = \hbar\omega_a|a\rangle\langle a| + \hbar\sum_{i=1}^N \omega_{b_i}|b_i\rangle\langle b_i|$ and $H_I^k = \hbar g\sum_{i=1}^N |a\rangle\langle b_i|\hat{a}e^{-i\Omega t} + \text{H.c.}$ Here $\hbar\omega_a, \hbar\omega_{b_i}$ are the energies of atomic states $|a\rangle$ and $|b_i\rangle$, with $i = 1\cdots N, g$ is the coupling rate between the atom and the field, and $\hat{a}$ is the photon annihilation operator. The model Hamiltonian describes a situation where the $N+1$-level atom is coupled to a single-mode cavity in a fan-shaped transition scheme. A more realistic model requires consideration of a multimode cavity coupled to an atom with multiple upper and lower hyperfine levels [30,31]. Such models can be reduced to an effective single-mode cavity and multilevel atom interactions [30] or can be directly described by generalized master equations of micromasers [32]. Atoms with fan-shaped degenerate level schemes are also studied from the perspective of generating large superposition states [25,33]. The central question for us here is the dependence of work and efficiency on the number of the superposed quantum states and we will only consider single upper level and a set of degenerate or nondegenerate lower levels for simplicity.

Analytically calculating the right-hand side of the Eq. (1), we find (see Appendix for details)

$$\begin{aligned}\dot{\rho}_{nn} = &-rg^2\{K_a\rho_{aa}[(n+1)\rho_{nn} - n\rho_{n-1,n-1}] \\ &+ \left(\sum_{i=1}^N K_{b_i}\rho_{b_ib_i} + \sum_{i<j} K_{ij}^{\phi_{ij}}|\rho_{b_ib_j}|\right) \\ &\times [n\rho_{nn} - (n+1)\rho_{n+1,n+1}]\},\end{aligned} \tag{2}$$

where the coefficients K_a, K_{b_i}, and $K_{ij}^{\phi_{ij}}$ depend on the atomic relaxation rate γ, atomic dephasing rate γ_ϕ, and detuning parameter $\Delta_i = \omega_{ab_i} - \Omega$, with $\omega_{ab_i} = \omega_a - \omega_{b_i}$ and $\omega_{b_ib_j} = \omega_j - \omega_i$, as well as the coherence parameters ϕ_{ij} and $|\rho^0_{b_ib_j}|$, by the relations given in the Appendix. Thus, we obtain the rate of change of average photon number

$$\dot{\bar{n}}_\phi = rg^2\{K_a\rho_{aa}(\bar{n}_\phi+1) - (R_{g_0} + R_{g_c})\bar{n}_\phi\}, \tag{3}$$

where $R_{g_0} = \sum_{i=1}^N K_{b_i}\rho_{b_ib_i}$ and $R_{g_c} = \sum_{i<j} K_{ij}^{\phi_{ij}}|\rho_{b_ib_j}|$.

The equation of motion for the evolution of population elements in the density matrix coincides with the thermalization dynamics of a resonator coupled to a heat bath. Accordingly, the coarse-grained dynamics effectively describes sequence of NLAP injected into the resonator as a mesoscopic ensemble of $N+1$ level atoms acting as a heat bath. The off-diagonal elements of the density matrix or the coherences can be kept vanishingly small to describe the steady-state approximately as a thermal equilibrium state. The corresponding effective

temperature can be determined by the modified detailed balance condition to reach such a quasiequilibrium state in Eq. (2) which gives

$$\frac{K_a}{R_{g_0}+R_{g_c}} = \exp\left(\frac{-\hbar\Omega}{kT_\phi}\right). \tag{4}$$

The detailed balance between the thermal reservoir at T_h and the photon gas in the resonator is broken but there is a modified detailed balance between the coherent atomic ensemble and the resonator photons. Accordingly, the resonator can reach a thermal equilibrium at a different temperature T_ϕ than T_h.

The steady state of the Eq. (3) yields the average photon number as

$$\bar{n}_\phi = \frac{\bar{n}}{1+\bar{n}\frac{R_{gc}}{K_a\rho_{aa}}}, \tag{5}$$

where $\bar{n} = (R_{g_0}/K_a\rho_{aa}-1)^{-1}$ is the average photon number in the absence of coherence. Using $\bar{n}_\phi = [\exp(\hbar\Omega/kT_\phi)-1]^{-1}$, we determine the effective cavity temperature as

$$T_\phi = \frac{T_h}{1+\bar{n}\frac{R_{gc}}{K_a\rho_{aa}}}, \tag{6}$$

by using high-temperature approximations $\bar{n}_\phi \approx kT_\phi/\hbar\Omega$ and $\bar{n} \approx kT_h/\hbar\Omega$ in Eq. (5).

Therefore, the efficiency of the photonic Carnot engine in the case of NLAP becomes

$$\eta_\phi = \eta_c - \frac{T_c}{T_h}\bar{n}\frac{R_{gc}}{K_a\rho_{aa}}, \tag{7}$$

where $\eta_c = 1-T_c/T_h$ is the Carnot efficiency. Note that for $T_c = T_h$ and $\eta_c = 0$ but η_ϕ could have a positive value for particular values of control parameters $\phi_1,\phi_2,\ldots,\phi_S$. In order to get further analytical results we will make some simplifying assumptions.

We focus on degenerate NLAP case to proceed analytically, for which $E_a = \Omega, E_{b_i} = 0, i = 1,\ldots,N, \omega_{ab_i} = \Omega, \Delta_i = 0, \omega_{b_ib_j} = 0$, and $K_a = 2N/\gamma^2$. In addition, we consider phase-locked equal amplitude coherences with $\phi_{ij} = \phi$ and $|\rho_{b_ib_j}| = \lambda$. Hence the coefficients in Eq. (2) become $K_{ij}^{\phi_{ij}} = 4\cos\phi/\gamma^2, R_{g_0} = 2NP_g/\gamma^2$, and $R_{g_c} = 2N(N-1)\cos\phi\lambda/\gamma\bar{\gamma}$, and hence Eq. (3) reduces to

$$\dot{\bar{n}}_\phi = 2\mu N[(P_e - P_g + N\xi\lambda)\bar{n}_\phi + P_e] - \kappa\bar{n}_\phi, \tag{8}$$

for $N \gg 1, \phi = \pi$, where $\mu = rg^2/\gamma^2, P_e = \rho_{aa} = \exp(-\beta E_a)/Z, P_g = \rho_{b_ib_i} = 1/Z$ with $Z = \exp(-\beta E_a)+N$. Here we introduced κ and ξ, with $|\xi| < 1$, as the decoherence rate due to the dissipation in the cavity and a phenomenological decoherence factor due to atomic dephasing, respectively [21]. While the dephasing factor is phenomenologically introduced in Ref. [21] we provide its rigorous microscopic derivation in the Appendix.

Steady-state solution of Eq. (8) yields an effective temperature given by $T_\phi = T_h/[1+F(T_h)]$ in the high-temperature limit where

$$F(T_h) = \frac{\bar{n}}{P_e}\left(-N\xi\lambda + \frac{\kappa}{2N\mu}\right), \tag{9}$$

with $\bar{n} = P_e/(P_g - P_e)$. For small coherence and decoherence terms in $F(T_h)$, an approximate expression can be written for the effective temperature

$$T_\phi = T_h\left(1 + N^2\xi\lambda\bar{n} - \frac{\kappa}{2\mu}\bar{n}\right). \tag{10}$$

This result shows that if the reduction of the magnitude of coherence due to dephasing is slower than the quadratic increase with N, then the multilevel coherence could be used to beat the decoherence induced by the cavity dissipation. The magnitude of coherence λ is limited by the positivity requirement of the density matrix as well as the thermal equilibrium requirement of the cavity field. The former condition requires $|\rho_{b_ib_j}| \leqslant (\rho_{b_ib_i}\rho_{b_jb_j})^{1/2}$ so $\lambda \leqslant 1/N$ for $N \gg 1$ as $\rho_{b_ib_i} \sim 1/N$ for $N \gg 1$. Accordingly, one can fix the coherence amplitude λ as a constant as long as it remains smaller than $1/N$ for the range of N values. For a realistic number of levels this is not a very restrictive condition. More severe limitation on λ is due to the quasiequilibrium condition of the photon gas. We will take $\lambda \sim 10^{-6}$ and consider $N \leqslant 40$ in our numerical examinations. In the classical asymptotical limit of $N \to \infty$ and then $\lambda \to 0$ as $1/N$ and hence the quadratic scaling reduces to a linear one for which the specific energy becomes a constant, as expected for classical systems. Mesoscopic systems in quantum regime are therefore necessary to exploit the quadratic scaling in the specific energy.

We note that the coarse-grained dynamics is designed on purpose to determine the steady state by rapid convergence using a numerically efficient dynamical equations. Analytical solution of the mean photon number dynamics for the degenerate case and with $\lambda = 0, \kappa = 0, \xi = 1$ gives

$$\bar{n}_\phi = \bar{n} - (\bar{n} - \bar{n}_0)\mathrm{e}^{-t/t_{\mathrm{th}}}, \tag{11}$$

where $t_{\mathrm{th}} = 1/2\mu N(P_g - P_e)$ is the thermalization time. We will first discuss the predicted analytical state states by the coarse-grained master equation in modern resonator settings and then examine the exact numerical description of the dynamics of the system to verify the analytical results in the subsequent subsections.

A. Analytical results for modern resonator systems

In the high-temperature limit ($T \gg \Omega$), the entropy change in the isothermal expansion stage is $\Delta S = k\Delta\Omega/\Omega$ and the heat input becomes $Q_{\mathrm{in}} = T_h\Delta S$. The work output at $T_h = T_c$ is found to be $W = Q_{\mathrm{in}}\eta$, where $\eta = \bar{n}(N^2\xi\lambda - \kappa/2\mu)$, respectively. In the superconducting circuit, microwave and optical resonators, it is estimated that $\kappa/2\mu\xi\lambda \sim 10$ [21]. N^2 should be replaced by $N(N-1)/2$ for smaller number of levels. Accordingly, by using five or more level quantum phaseonium fuel, the working fluid can beat quantum decoherence to harvest positive work.

In Fig. 3, we plot the work output and efficiency of the photonic Carnot engine with degenerate NLAP fuel, depending on the number of quantum coherent levels. We consider N-independent as well as N-dependent scaling models [34] for the decoherence factor and take $\xi = \exp(-x)$ in Figs. 3(a) and 3(b), $\xi = \exp(-Nx)$ in Figs. 3(c) and 3(d), and $\xi = \exp(-N^2x)$ in Figs. 3(e) and 3(f), where $x = \gamma_\phi/\gamma$ as shown in the Appendix. The plots are given for the circuit quantum electrodynamics (QED) parameters in Ref. [21]. We consider larger atomic dephasing rates than the typical values

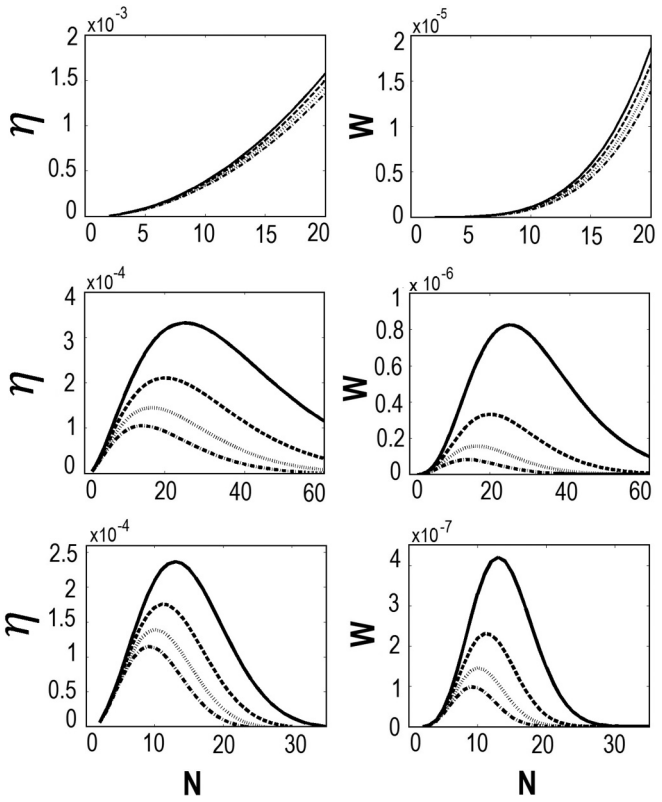

FIG. 3. Extracted work (W) and efficiency (η) of photonic Carnot engine, with $N+1$ level atom phaseonium (NLAP) fuel, depending on the number of degenerate coherent ground-state levels N, for different decoherence factor models [(a) and (b)] $\xi = \exp(-x)$ and [(c) and (d)] $\xi = \exp(-Nx)$. [(e) and (f)] $\xi = \exp(-N^2x)$, where $x = \gamma_\phi/\gamma$. Coherence parameter is $\lambda = 10^{-6}$ and the initial thermal coherent atomic temperature is $T_h = 4$ in units of $\hbar\Omega/k_B$. x values are 0.15, 0.1, 0.05, and 0.001 for (a) and (b); 0.14, 0.12, 0.1, 0.08 for (c) and (d); and 0.012, 0.01, 0.008, 0.006 for (e) and (f) for the dashed-dotted, dotted, dashed, and solid lines, respectively. The plots are given for the circuit QED parameters in Ref. [21]. The quantities $g = 0.01$, $r = 1 \times 10^{-4}$, $\kappa = 6.25 \times 10^{-4}$, and $\gamma = 5 \times 10^{-6}$, which are the coupling coefficient to the cavity field, atomic injection rate, cavity loss term, and atomic decay, respectively, are dimensionless and scaled with the resonance frequency $\Omega \sim 10$ GHz. η is dimensionless, and W is dimensionless and scaled with Ω.

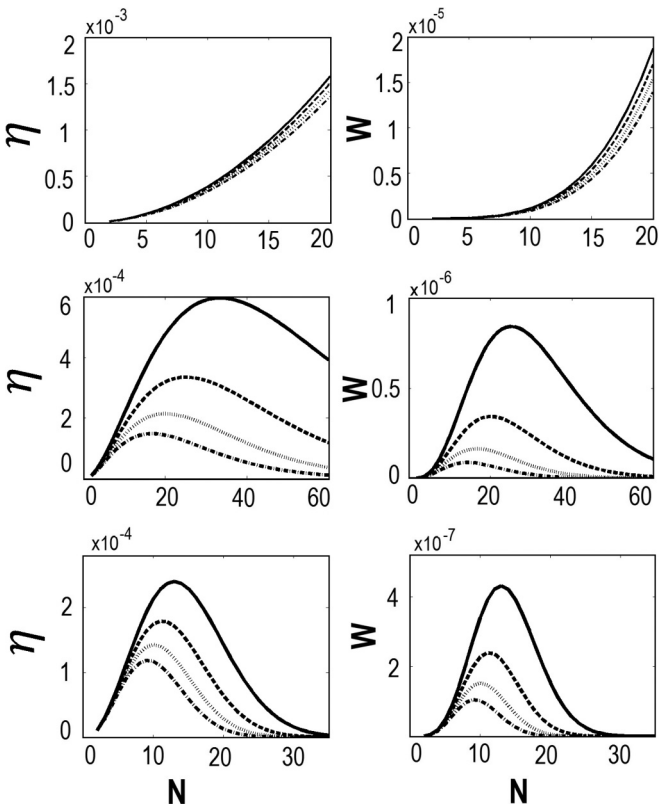

FIG. 4. Extracted work (W) and efficiency (η) of microwave resonator photonic Carnot engine, with $N+1$ level atom phaseonium (NLAP) fuel, depending on the number of degenerate coherent ground-state levels N for different decoherence factors [(a) and (b)] $\xi = \exp(-x)$, [(c) and (d)] $\xi = \exp(-Nx)$, and [(e) and (f)] $\xi = \exp(-N^2x)$, where $x = \gamma_\phi/\gamma$. The coherence parameter is $\lambda = 10^{-6}$ and the initial thermal coherent atomic temperature is $T_h = 4$ in units of $\hbar\Omega/k_B$. x values are 0.1, 0.15, 0.05, 0.001 for (a) and (b); 0.12, 0.1, 0.08, 0.06 for (c); 0.14, 0.12, 0.1, 0.08 for (d); and 0.012, 0.01, 0.008, 0.006 for (e) and (f) for the dashed-dotted, dotted, dashed, and solid lines, respectively. The parameters $g = 9.21 \times 10^{-7}$, $r = 6.47 \times 10^{-5}$, $\kappa = 1.96 \times 10^{-8}$, and $\gamma = 9.54 \times 10^{-10}$ are the atom-field coupling coefficient, atomic injection rate, cavity loss term, and atomic decay, respectively. They are dimensionless and scaled with the typical resonance frequency is $\Omega = 51$ GHz [35]. η is dimensionless, and W is dimensionless and scaled with Ω.

to demonstrate its limiting effect on W and η. The plots indicate that even when there is large dephasing, which can increase with N linearly or quadratically, W and η can retain their quadratic power law with N up to a critical N.

Similar results are found for the cases of optical and microwave cavities. We see in Figs. 4(a) and 4(b) and Figs. 5(a) and 5(b) that when dephasing is independent of N, the work output and efficiency increases quadratically with the number of coherent levels. If the dephasing rate is increasing linearly with N as in Figs. 4(c) and 4(d) and Figs. 5(c) and 5(d), or if it is increasing quadratically with N as in Figs. 4(e) and 4(f) and Figs. 5(e) and 5(f), then the work output and efficiency of the photonic engine is enhanced quadratically with the number of coherent levels only up to critical N, beyond which the work output and efficiency decays exponentially due to the dominating effect of decoherence.

B. Numerical verification of the theory

In order to perform a faithful numerical simulation of a typical setup described in theory, we investigate the injection process in detail. We assume a regular atomic injection of Rydberg atoms into a Fabry-Perot cavity [37] with an atomic interaction time τ with the cavity field and an empty cavity time τ_0 such that $1/r = \tau + \tau_0$, where r is the injection rate. During the time interval τ, the Hamiltonian is

$$H = \omega_a|a\rangle\langle a| + \Omega\hat{a}^\dagger\hat{a} + g\left(\sum_{i=1}^{N}|a\rangle\langle b_i|\hat{a} + \text{H.c.}\right), \quad (12)$$

while for the time interval τ_0, $H = \Omega\hat{a}^\dagger\hat{a}$ ($\hbar = 1$ and $\omega_{b_i} = 0$ for degenerate ground-state levels).

We choose injection time $1/r = 1/(N_{\text{ex}}\kappa)$, where κ is the cavity decay rate and N_{ex} is the number of atoms kicking the

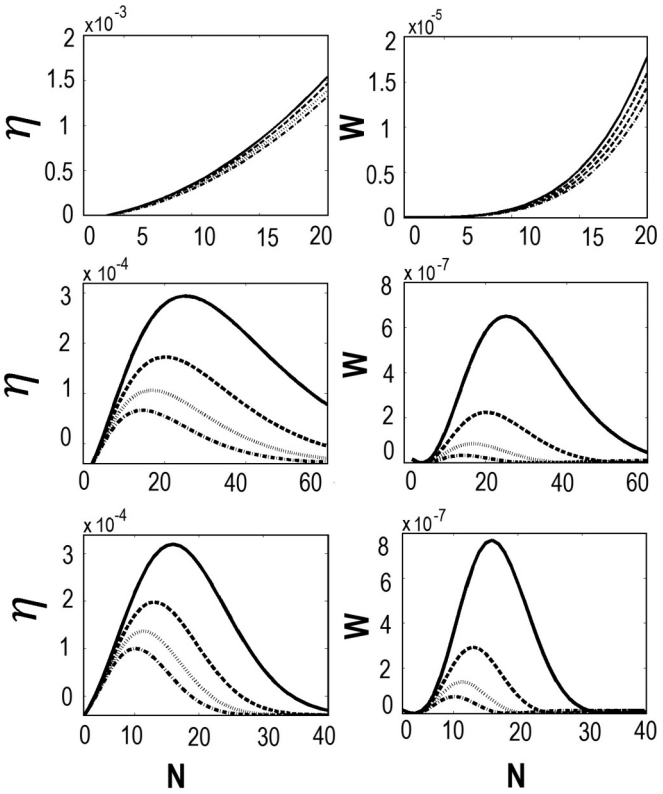

FIG. 5. Extracted work (W) and efficiency (η) of optical resonator photonic Carnot engine, with $N+1$ level atom phaseonium (NLAP) fuel, depending on the number of degenerate coherent ground-state levels N for different decoherence factors [(a) and (b)] $\xi = \exp(-x)$, [(c) and (d)] $\xi = \exp(-Nx)$, and [(e) and (f)] $\xi = \exp(-N^2x)$, where $x = \gamma_\phi/\gamma$. Coherence parameter is $\lambda = 10^{-6}$ and the initial thermal coherent atomic temperature is $T_h = 4$ in units of $\hbar\Omega/k_B$. The x values are 0.15, 0.1, 0.05, 0.001 for (a) and (b); 0.14, 0.12, 0.1, 0.08 for (c) and (d); and 0.01, 0.008, 0.006, 0.004 for (e) and (f) for the dashed-dotted, dotted, dashed, and solid lines, respectively. The parameters $g = 6.28 \times 10^{-7}$, $r = 8 \times 10^{-5}$, $\kappa = 2.86 \times 10^{-7}$, and $\gamma = 4.68 \times 10^{-8}$ are the coupling frequency to the cavity field, atomic injection rate, cavity loss term, and atomic decay, respectively. They are dimensionless and scaled with the typical resonance frequency is $\Omega = 350$ THz [36]. η is dimensionless, and W is dimensionless and scaled with Ω.

cavity field in the photon lifetime. The time elapsed when cavity is empty τ_0 can be related to the interaction time such that $\tau_0 = N_{\rm em}\tau$. Thus, we can write $1/r = \tau(1 + N_{\rm em})$. Here, $N_{\rm em}$ is a factor introduced to measure τ_0 in terms of τ so $N_{\rm em} = 1/(N_{\rm ex}\kappa\tau) - 1$.

We solve the master equation by numerical methods and compare the results with the developed theory. We use the QuTip package [38] in PYTHON software to solve the master equation. We perform single atomic injection in two steps. First step is the atom-cavity field interaction (during τ) and the second one is the free cavity field evolution (during τ_0). The master equation for the first step is written under Markov and Born-Markov approximations as [39]

$$\dot\rho = -i[H,\rho] + \gamma\sum_m^{N+1}\mathcal{L}[L_m^\gamma] + \frac{\gamma_\phi}{2}\sum_n^{N}\mathcal{L}[L_n^\phi], \qquad (13)$$

where last two terms stand for pure spontaneous emission and pure dephasing [40–43], respectively. Here $\mathcal{L}[x] = (2x\rho x^\dagger - xx^\dagger\rho - \rho x^\dagger x)/2$ is a Liouvillian superoperator in Lindblad form and $L_m^\gamma = |r\rangle\langle\alpha_m|, L_n^\phi = |b_n\rangle\langle b_n|$. We include an auxiliary state $|r\rangle$ to the atomic state space to model the decay of the excited and the lower levels. Presence of $|r\rangle$ is not altering the initial phaseonium state. The auxiliary state is unpopulated and at the lower level energy. Its use allows for faithful simulation of the excited state and the degenerate ground-state ($\alpha_m = a, b_1, \ldots, b_N$) decay equations in Eq. (A19). This decay model is already used in the original master equation developed for the two-level phaseonium engine [6]. Different decay models, for example, decay of excited level to the lower levels are employed for other systems such as many atom superradiant Otto engine [20] and similar effect of beating decoherence with scaling up coherence is found. The present contribution discusses the original photo-Carnot engine [4] as well as the objection to its feasibility due to dephasing, phenomenologically described by factor ξ [21]. Our introduction of γ is an additional decoherence channel not included in Ref. [21]. We have found that γ_ϕ can be analytically expressed in terms of ξ (see Appendix for details). The microscopical master equation approach describes the original photo-Carnot engine coarse-grained master equations both with [21] and without [6] dephasing and generalizes them to the multilevel case, as our mesoscopic master equation, Eq. (2), does analytically.

In the second step, cavity decay (κ) is present during the time interval τ_0 in accordance with the key assumptions of micromaser theory [24] and the corresponding master equation is

$$\dot\rho = -i[H,\rho_f] + \kappa\mathcal{L}[\hat a]. \qquad (14)$$

In Fig. 6, we present the thermalization process of the cavity field depending on different $N_{\rm ex}$ values by depicting the photon number versus scaled time. Physical parameters [21] are given in the figure caption consistent with the Rydberg atoms in a superconducting Febry-Perot cavity [37]. For low values of $N_{\rm ex}$ which correspond to large $N_{\rm em}$, we have zigzag-like curves and for high values of $N_{\rm ex}$ we have smoother lines. The average photon number $\bar n_\phi$ converges to the theoretical value for $N_{\rm em} = 12 \times 10^3$. Thermalization time is much longer than the convergence rate of coarse-grained master equation and the microscopic exact method is much more costly numerically.

In Figs. 7(a) and 7(b), we express the effect of the number of degenerate atomic ground-state levels N of the coherent atoms against the dephasing and the cavity loss mechanisms. Horizontal dotted and dotted-dashed lines are the analytical values of average photon numbers($\bar n_\phi, \bar n$) of the no loss case for each N. In Fig. 7(a) when decoherence channels are open, average photon number saturates below the analytical values for $N = 2$ in accordance with the argument that 2LAP phaseonium cannot beat decoherence [21]. The average photon number exceeds $\bar n$ for $N = 4$ in Fig. 7(b) by keeping all the other parameters the same. Thus, we show that the decoherence can be beaten by using higher N. To make the effect more visible in the figures, we take larger coherence magnitude, $\lambda = 10^{-3}$.

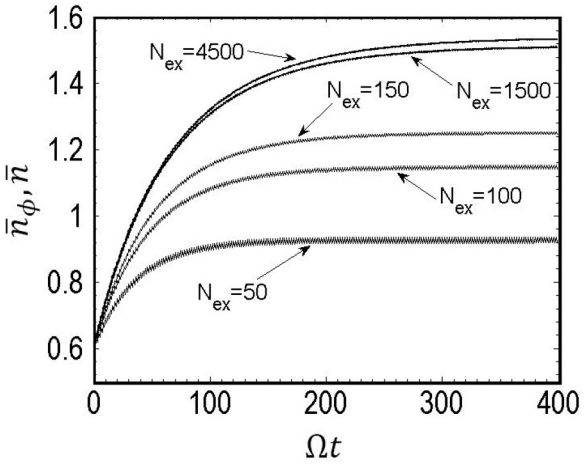

FIG. 6. Time evolution of average photon number during thermalization process of PCE field while regular injection of 2LAP depending on different $N_{\rm ex}$ parameters. $N_{\rm ex}$ values are 4500, 1500, 150, 100, and 50 in decreasing order for the upper to lower curves, respectively. The coherence parameter is $\lambda = 10^{-3}$, the initial field temperature $T_f = 1$, and the temperature of the thermal coherent atoms is $T_h = 2$ in units of $\hbar\Omega/k_B$. The resonant field frequency is $\Omega = 51$ GHz, cavity quality factor is $Q = 2 \times 10^{10}$, atom cavity field interaction time is $\tau = 10$ μs, atom decay rate is $\gamma = 33.3$ Hz, atom dephasing rate is $\gamma_\phi = 3.3$ Hz, and the atom cavity field coupling is $g = 50$ kHz. Time is dimensionless and scaled with Ω.

We also compare the consistency of effective field temperature $T_{\rm eff}$, harvested work (W), and efficiency (η) versus N in Fig. 8 between developed analytical and numerical results when dissipation channels open. We observe a good consistency between numerical and theoretical results in steady state.

C. Preparation of the NLAP and its energy cost

Typical methods to generate quantum superposition states, such as pulse area, adiabatic passage, or STIRAP techniques [25,26], utilize optical pulses interacting with the atomic system to transfer an initial atomic state to a target one. The initial and target quantum states are known and hence one can easily determine the required unitary transformation between them. Physical implementation of the required propagator is, however, a much more challenging problem than the calculation of the transformation matrix. An efficient strategy to synthesize the transformation matrix is to decompose it into a product of matrices, representing interacting steps that can be implemented by using optical pulses coupled to the atom.

Let us briefly describe a few more details of the physical implementation of the transformation matrix that we shall consider (see Refs. [28,29] and the references therein). The atom consists of N degenerate ground states coherently coupled to a common excited ancilla state by resonant or nearly resonant pulsed external laser fields in a fan shaped N-pod transition scheme. The temporal profiles and the detunings from the atomic resonance of the pulses are the same; but their amplitudes and the phases can differ. Nonzero detuning allows for a more general transformation matrix. Using femtosecond pulses is advantageous to eliminate population losses and to reduce decoherence effects on such short interaction times;

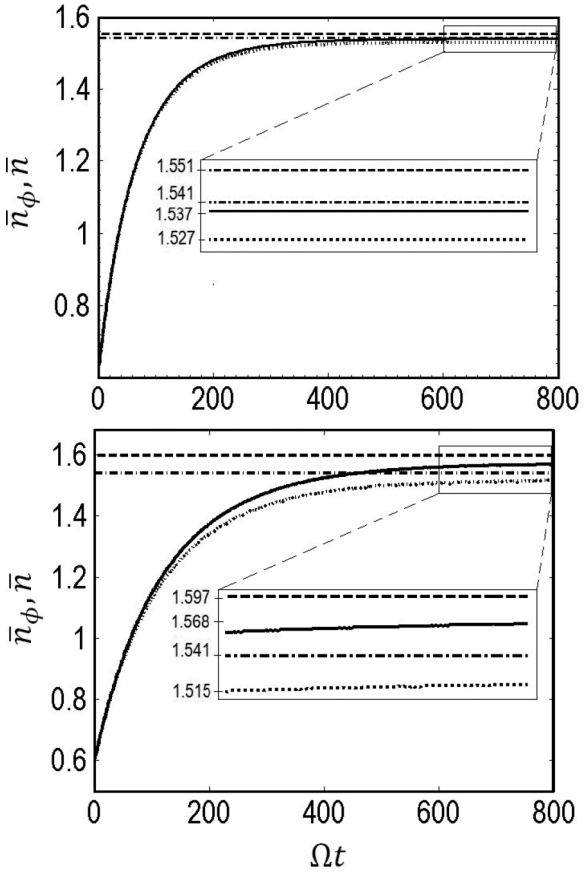

FIG. 7. Comparison of time evolution of average photon number in presence of thermal and coherent atom injection with $N = 2$ (top figure) and $N = 4$ (bottom figure). The horizontal dashed and dashed-dotted lines stands for the analytical $\bar{n}_\phi$ and $\bar{n}$ values in absence of loss mechanisms. Solid and dotted lines stands for time evolution of $\bar{n}_\phi$ and $\bar{n}$, respectively, in presence of dissipation channels. $N_{\rm ex} = 4000$ for both subplots corresponding to $\tau_0 = 90$ μs. Insets magnifies the lines between $\Omega t = 600$ and $\Omega t = 800$. All the remaining parameters are the same with that of Fig. 6. Time is dimensionless and scaled with Ω.

besides, pulse shapes and areas can be controlled to a high degree of accuracy. It is sufficient to use a few tunable lasers and split their fields using beam splitters to further ensure identical pulse profiles, which are typically hyperbolic secant or Gaussian. Polarizers can be used to selectively couple atomic states to the laser fields. An interaction step is achieved by simultaneously coupling N coincidence pulses in fan-shaped transition scheme to the $N + 1$-level atom. This is repeated sequentially by the train of set of laser pulses. The process ends when the initial state is navigated into the target state by the product of the propagators of interaction steps. Relative to other pulse area or adiabatic transfer schemes, which require N^2 operations, the coincidence pulse technique needs fewer, N, operational steps.

An arbitrary N dimensional unitary matrix $\mathbf{U}(N)$ can be decomposed into so-called N-generalized quantum Householder reflection (QHR) matrices or $N - 1$ standard QHRs and a phase gate [28,29]. A generalized QHR is defined by

$$\mathbf{M}(\nu;\phi) = \mathbf{I} + (e^{i\phi} - 1)|\nu\rangle\langle\nu|, \tag{15}$$

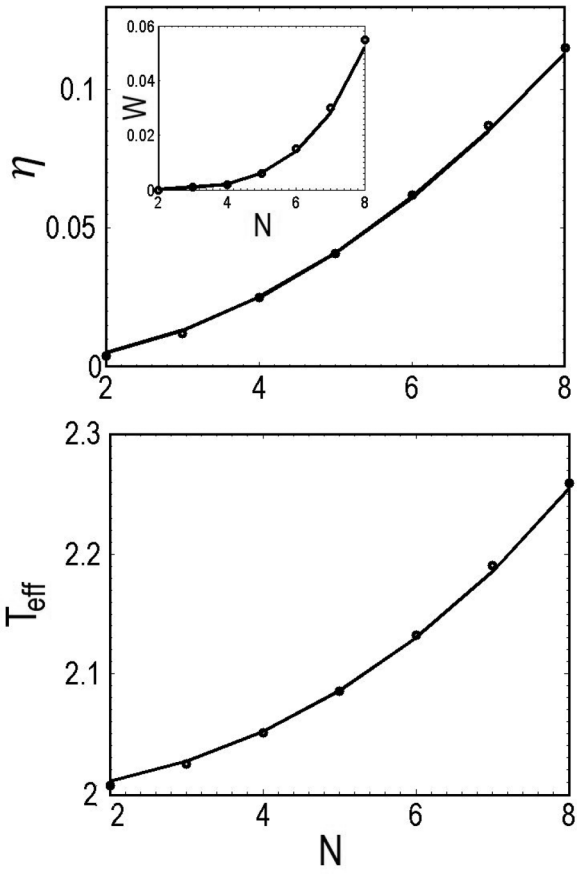

FIG. 8. Comparison of numerical results (black circles) with developed theory (solid line) of efficiency η (top figure), harvested work W (inset), and effective field temperature $T_{\rm eff}$ (bottom figure), respectively, depending on the number of degenerate ground-state levels N. $N_{\rm ex} = 12 \times 10^3$ and corresponding $\tau_0 = 2.01\,\mu$s. All the remaining parameters are the same as in Fig. 6. η is dimensionless, $T_{\rm eff}$ and W are dimensionless and scaled with Ω.

where $\mathbf{I}$ is the identity operator and the $|\nu\rangle$ is the normalized column vector with dimension N, the same with the number of the pulses, and ϕ is an arbitrary phase factor. The decomposition of $\mathbf{U}(N)$ in terms of generalized QHRs can be written as

$$\mathbf{U} = \mathbf{M}(\nu_1;\phi_1)\mathbf{M}(\nu_2;\phi_2)\ldots\mathbf{M}(\nu_N;\phi_N). \tag{16}$$

For $\phi = \pi$, Eq. (15) reduces to $\mathbf{M} = \mathbf{I} - 2|\nu\rangle\langle\nu|$, which is the standard QHR. The interaction represented by each Householder matrix can be described by a propagator which can be determined by the Morris-Shore transformation [27].

Our N+1 level atom coupled to N optical pulses in a fan-shaped transition scheme, or so-called N-pod model, is a generic model that is used to discuss generation of arbitrary multilevel superposition states. Under the Morris-Shore transformation, the lower levels of the atom are grouped into a single bright level coupled to an effective single pulse and $N-1$ dark levels uncoupled from the optical pulses. The propagator is then easily determined in this Morris-Shore basis. Back-transformation to the original basis gives the full propagator or the generalized QHR matrix. Both the number of QHR steps and the number of pulses used in each step are in the order of N, and therefore the total number of pulses to be used to generate the target state would be in the order of N^2. This shows that the energetic cost of preparation of the target state scales with N^2, same with the work and efficiency scaling in the corresponding photonic Carnot engine.

The preceding discussion is applicable to the case of mixed states as well, for which the normalized vectors of generalized QHRs are defined as [28]

$$|\nu_i\rangle = \frac{1}{e^{-i\phi_i} - 1}\sqrt{\frac{2\sin(\phi/2)}{|1-u_{ii}|}}(|u_i\rangle - |e_i\rangle). \tag{17}$$

Here u_i is the $i^{\rm th}$ column of $\mathbf{U}(N), |e_i\rangle = [0,\ldots,1^{i\rm th},\ldots,0]^T$ and ϕ is an arbitrary phase where $\phi_i = 2\arg(1-u_{ii}) - \pi$. It is shown that for an N-pod system any standard QHR $\mathbf{M}(\nu)$ can be realized by single pulses with an rms pulse area $A = 2\pi$ [29]. The corresponding unitary transformation can only link the mixed states with the identical dynamical invariants. In our case we consider initial thermal states out of a hohlarum transformed to a final state with small coherences. The initial and final states would then possess different spectral decompositions so they cannot be unitarily connected. A resolution to this is suggested to exploit decoherence channels such as spontaneous emission or pure dephasing in combination with the unitary transformation [28,29]. We will not follow this route but use an alternative, which allows for a fully unitary procedure to generate desired coherences. As the coherences contribute additively, to exploit their scaling advantage we do not need an exact state but an approximate one would be sufficient. Accordingly, we can simply consider an approximate approach and do not specify an exact value for the coherences. We only need to keep them small enough to ensure slightly out of thermal equilibrium final state. We illustrate our strategy for $N = 2$ case and suggest that in principle larger NLAP can be generated by straightforward extension of this technique. Unitarity of our procedure also makes the details of generation process immaterial for the cost estimation. The cost would be the same for other unitary equivalent processes to generate same states.

The initial state of the atom from the hohlarum at T_h is the thermal density matrix

$$\rho_{\rm th} = \frac{1}{Z}e^{-\beta H} = \sum_{n=1}^{N+1} P_n|\Psi_n\rangle\langle\Psi_n|, \tag{18}$$

where $\beta = 1/k_B T_h$ is the inverse temperature ($k_B = 1$) and $Z = {\rm Tr}e^{-\beta H}$ is the partition function, with $H = \sum_{i=1}^{N+1}\hbar\omega_i|i\rangle\langle i|$ being the atomic Hamiltonian. Taking $N = 2$ and $T_h = 2$, we find $\rho_{\rm th} = {\rm diag}(0.327,0.384,0.384)$. Target density matrix ρ_c is taken to be

$$\rho_c = \begin{pmatrix} 0.327 & 0 & 0 \\ 0 & 0.384 & 0.000001 \\ 0 & 0.000001 & 0.384 \end{pmatrix}, \tag{19}$$

where the off-diagonal elements between degenerate ground-state levels are taken real and much smaller than the diagonal elements that are equal to those of the $\rho_{\rm th}$. The initial and final density matrices have distinct dynamical invariants in their spectral decompositions and hence they cannot be linked by a coherent evolution. Let us assume,

however, an approximate link such that $\rho_c \approx \mathbf{U}\rho_{\rm th}\mathbf{U}^\dagger$. The unitary transformation $\mathbf{U}$ can be determined from the matrix that diagonalize ρ_c and found to be

$$\mathbf{U} = \begin{pmatrix} 1 & 0 & 0 \\ 0 & -0.707 & 0.707 \\ 0 & 0.707 & 0.707 \end{pmatrix}. \tag{20}$$

Writing $\tilde{\rho}_c = \mathbf{U}\rho_{\rm th}\mathbf{U}^\dagger$, the fidelity between ρ_c and $\tilde{\rho}_c$ is determined by $\mathcal{F}(\rho_c,\tilde{\rho}_c) = |Tr\sqrt{\sqrt{\rho_c}\tilde{\rho}_c\sqrt{\rho_c}}|^2$ and found be $\mathcal{F}(\rho_c,\tilde{\rho}_c) \simeq 1$. Thus, $\tilde{\mathbf{U}}$ can be approximately be used as the unitary operator linking the initial and the target density matrices.

$\tilde{\mathbf{U}}$ can be synthesized by using two standard QHRs and a phase gate as

$$\tilde{\mathbf{U}} = \mathbf{M}(\nu_1;\phi_1)\mathbf{M}(\nu_2;\phi_2)\mathbf{M}(\nu_3;\phi_3), \tag{21}$$

where $\phi_1 = \phi_2 = \phi_3 = \pi$ and $\mathbf{M}(\nu_3;\phi_3) = \Phi(0,0,\Phi_3)$ is a one-dimensional phase gate. By using Eq. (17) one finds the normalized column vectors to be $|\nu_1\rangle = [0,0,0]^T, |\nu_2\rangle = [0,0.924, -0.383]^T$. The example for $N = 2$ here illustrates the basic principles to generate arbitrary NLAP. One can use N pulses for each $N-1$ standard QHRs and a phase gate to synthesize a unitary transformation matrix, which is the diagonalization matrix of a quasiequilibrium thermal state at T_h with small coherences. When the pulses applied to the actual atom out of hohlarum at T_h, the final state will be approximately the same with the target state used to determine the properties of the pulses.

We can now estimate the energy cost U_c of generating ρ_c using $U_c = N^2 U_p$, where N^2 is the total number of pulses used in the QHR technique and U_p is the energy of a single pulse. U_p can be determined from the pulse area A as in Ref. [20]. For a square pulse of duration τ_p and amplitude E_p we have $A = dE_p\tau/\hbar$, where d is the magnitude of the dipole moment

$$d = \sqrt{\frac{3\pi\epsilon_0\hbar c^3\gamma}{\Omega^3}}, \tag{22}$$

where ϵ is the vacuum permittivity and c is the speed of light. Taking the pulse area $A = 2\pi$ we find

$$E_p = \frac{2\pi\hbar}{\tau_p}\sqrt{\frac{\Omega^3}{3\pi\epsilon_0\hbar c^3\gamma}}. \tag{23}$$

The intensity of the pulse is given by $I_p = c\epsilon_0|E_p|^2/2$. The pulse energy in a beam of radius r_b can be estimated by $U_p = \pi r_b^2 I_p \tau_p$. Using $\Omega = 2\pi c/\lambda$ and $\zeta = \lambda/2\pi r_b$, where λ and ζ are the wavelength of the optical field and the radial beam divergence, respectively, we find

$$U_p = \hbar\Omega\frac{\pi^2}{6}\frac{1}{\tau_p\gamma}\frac{1}{\zeta^2}. \tag{24}$$

Taking $1/\tau_p\gamma \sim 2$ and $\zeta \sim 0.5$ [20], we find $U_p \sim 12\hbar\Omega$.

The total energy cost to reach steady state per cycle is $U_{\rm ss} = mU_c = mN^2U_p$, where $m = r\Delta t_s$. Here m is the number of atoms needed for thermalization, r is the injection rate, and Δt_s is the time elapsed to reach the steady state. In our results we have found that the harvested work per cycle is much less than the resonance energy, $W \ll \hbar\Omega$, thus the generation cost of NLAP fuel is several orders of magnitude larger than the harvested work $U_{\rm ss} \gg W$, which confirms that the second law of thermodynamics obeyed in a photonic Carnot engine with NLAP. The generation cost is not included in the thermodynamic efficiency but it can be a significant figure of merit in the round-trip efficiency. To make such photonic Carnot engines more appealing for certain applications, it is necessary to increase their round-trip efficiency as well. For that aim one could consider the cases of larger compression ratios ($\Delta\Omega \gg \Omega$) and high operation temperatures ($k_B T_h \gg \hbar\Omega$). Our focus here is on the discussion if such engines can operate under decoherence. Despite the negative conclusions for a two-level phaseonium case [21], we have found that larger phaseonium fuel allows for operational photonic Carnot engines. The question of how to increase their round-trip efficiency requires further analysis which is beyond the scope of present contribution.

IV. CONCLUSIONS

Summarizing, we examined scaling of work and efficiency of a quantum heat engine with the number of quantum resources. Specifically, we considered a photonic Carnot engine with a multilevel phaseonium quantum fuel. We derived a generalized master equation for the cavity photons, which forms the working fluid of the engine, and determined the steady-state photon number to calculate the work output and thermodynamic efficiency. We find that they scale quadratically with the number of quantum coherent levels N.

The role of the quantum coherence in multilevel phaseonium fuel is the same as the original two-level phaseonium proposal [4]. It breaks the detailed balance between the heat reservoir and the cavity field. A modified detailed balance condition can be established between an effective heat reservoir, at an effective higher temperature than the physical heat reservoir, and the cavity field. Accordingly, the resonator field can reach a quasithermal equilibrium at a higher temperature than the heat reservoir. This allows for operating a Carnot cycle using a single heat bath, and an atomic coherence reservoir, which could be seen as an apparent violation of the Carnot bound. However, the energetic cost of coherence preparation as well as the modified detailed balance condition ensure that the thermodynamical laws are not violated. Our generalization of N level phaseonium fuel reveals that quantum coherent contribution to the heat reservoir temperature scales quadratically with N, which is translated into quadratic scaling of the specific energy of the multilevel phasenonium fuel with the number of coherent levels.

We examined the case of degenerate levels to get analytical results and to examine scaling laws against decoherence due to cavity dissipation and atomic dephasing. We verified our analytical results with detailed numerical methods and have shown consistency of coarse-grained analytical results with the microscopical numerical approach. Generation of multilevel phaseonium fuel using a Morris-Shore transformation-determined quantum Householder reflection technique as well as its cost are examined. Using typical parameters in modern resonator systems, such as circuit QED, our calculations reveal that decoherence due to cavity dissipation could be overcome by the multilevel quantum coherence even in the presence of a large dephasing rate. If the dephasing rate increases with N,

then work and efficiency can still overcome the decoherence and retain their N^2 scaling up to a critical number of coherent levels.

ACKNOWLEDGMENTS

The authors warmly thank N. Allen, A. Imamoglu, and I. Adagideli for illuminating discussions. The authors acknowledge support from Koç University and Lockheed Martin Corp. University Research Agreement.

APPENDIX

We generalize the micromaser mesoscopic master equation treatment [6] applied for a three-level phaseonium engine [4] to a multilevel case. In the NLAP model, the Hamiltonian of the whole system is $H = H_0 + H_I^k$ where label k implies an injected k^{th} arbitrary atom. We adopt the notation of Ref. [44] for the Hamiltonian and relevant quantities. Here $H_0 = \hbar\omega_a|a^k\rangle\langle a^k| + \hbar\sum_{i=1}^{N}\omega_{b_i}|b_i^k\rangle\langle b_i^k|$ and

$$H_I^k = \hbar g\sum_{i=1}^{N}|a^k\rangle\langle b_i^k|\hat{a}e^{-i\Omega t} + \text{H.c.} \tag{A1}$$

in the interaction picture where ω_1,ω_{b_i} are atomic energy levels, g is the atom-field coupling coefficient, and Ω is the single-mode cavity frequency. Here we assume all levels coupled to the excited one with the same coefficient g. The equation of motion of overall system is

$$\dot{\rho} = -\frac{i}{\hbar}[H,\rho] + \mathcal{L}_A[\rho] + \mathcal{L}_f[\rho], \tag{A2}$$

where $\mathcal{L}_A[\rho]$ and $\mathcal{L}_f[\rho]$ are the Liouvillian superoperators expressed in the main text corresponding to atomic and field degrees of freedom, respectively.

The equation of motion of the radiation field which is the working substance of the heat engine can be found by tracing out the atomic part as

$$\dot{\rho}_{nn} = -\frac{i}{\hbar}\sum_k(\text{Tr}_{\text{at}}[H^k,\rho^k]_{nn}) + \text{Tr}_{\text{at}}\mathcal{L}_A[\rho]_{nn} + \text{Tr}_{\text{at}}\mathcal{L}_f[\rho]_{nn}, \tag{A3}$$

where $\dot{\rho}_{nn} = \langle n|\dot{\rho}|n\rangle$. Here $[H,\rho]_{nn} = \langle n|(H\rho - \rho H)|n\rangle = \sum_m\langle n|H|m\rangle\langle m|\rho|n\rangle - \sum_m\langle n|\rho|m\rangle\langle m|H|n\rangle = \sum_m(H_{nm}\rho_{mn} - \rho_{nm}H_{mn})$. In micromaser theory, due to the short atom-cavity interaction time, the last term, the cavity decay, is usually ignored when the atom is inside the cavity. The second term is treated perturbatively and will be considered for zeroth order in g. Here we will keep it but assume it can be treated independently. One may write the partial trace operation over atomic degrees of freedom for a random single atom as

$$\text{Tr}_{\text{at}}[H,\rho]_{nn} = \sum_\alpha\langle\alpha,n|[H,\rho]|\alpha,n\rangle = \langle an|[H,\rho]|an\rangle + \sum_{i=1}^{N}\langle b_i n|[H,\rho]|b_i n\rangle, \tag{A4}$$

where α are the atomic basis as expressed on the right-hand side. Each term of Eq. (A4) can be calculated by using the selective rules of the Hamiltonian between certain levels n and m; for instance, by inserting it for the first term of Eq. (A4) we have

$$\begin{aligned}\langle an|[H,\rho]|an\rangle &= \langle an|(H\rho - \rho H)|an\rangle \\ &= \sum_{\alpha' m}\{\langle an|H|\alpha' m\rangle\langle\alpha' m|\rho|an\rangle \\ &\quad - \langle an|\rho|\alpha' m\rangle\langle\alpha' m|H|an\rangle\} \\ &= \sum_{\alpha' m}\{H_{an,\alpha' m}\rho_{\alpha' m,an} - \rho_{an,\alpha' m}H_{\alpha' m,an}\}.\end{aligned} \tag{A5}$$

H_I is the Hamiltonian Eq. (A1) to be inserted into Eq. (A5) which can be written as

$$H_I = \hbar g\hat{R}_+\hat{a}e^{-i\Omega t} + \hbar g\hat{R}_-\hat{a}^\dagger e^{i\Omega t}, \tag{A6}$$

where $\hat{R}_+ = \sum_{i=1}^{N}|a\rangle\langle b_i|$ and $\hat{R}_- = \hat{R}_+^\dagger$. Expressing the terms of Eq. (A5) conveniently, we write

$$\begin{aligned}(\hat{R}_+)_{a\alpha'} &= \langle a|(|a\rangle\langle b_1| + \cdots + |a\rangle\langle b_N|)|\alpha'\rangle \\ &= (\delta_{b_1\alpha'} + \cdots + \delta_{b_N\alpha'})\end{aligned} \tag{A7}$$

and $(\hat{R}_-)_{a\alpha'} = 0$. Besides, $\hat{a}_{nm} = \langle n|\hat{a}|m\rangle = \sqrt{m}\langle n||m-1\rangle = \sqrt{m}\delta_{n,m-1}$. Substituting these terms into the first part of Eq. (A5) we have $\sum_{\alpha' m}\{H_{an,\alpha' m}\rho_{\alpha' m,an}\} = \hbar g e^{-i\Omega t}\sqrt{n+1}(\rho_{b_1 n+1,an} + \cdots + \rho_{b_N n+1,an})$. The second part of Eq. (A5) is simply the complex conjugate. Hence the first term of Eq. (A4) is

$$\langle an|[H,\rho]|an\rangle = \hbar g e^{-i\Omega t}\sqrt{n+1}\sum_{i=1}^{N}\rho_{b_i n+1,an} - \text{c.c.} \tag{A8}$$

The second term of Eq. (A4) would be calculated by similar considerations. We can write $\langle b_i n|[H,\rho]|b_i n\rangle = \sum_{\alpha' m}\{H_{b_i n,\alpha' m}\rho_{\alpha' m,b_i n}\}$. In this case $(\hat{R}_+)_{b_i\alpha'}=0, (\hat{R}_-)_{b_i\alpha'} = \langle a||\alpha'\rangle = \delta_{a\alpha'}$, and $\hat{a}_{nm}^\dagger = \langle n|\hat{a}^\dagger|m\rangle = \sqrt{m+1}\langle n||m+1\rangle = \sqrt{m+1}\delta_{n,m+1}$. Then $\langle b_i n|[H,\rho]|b_i n\rangle = \hbar g e^{i\Omega t}\sqrt{n}\rho_{an-1,b_i n} - \text{c.c.}$ and, finally, the second term of Eq. (A4) becomes

$$\sum_{i=1}^{N}\langle b_i n|[H,\rho]|b_i n\rangle = \hbar g e^{i\Omega t}\sqrt{n}\sum_{i=1}^{N}\rho_{an-1,b_i n} - \text{c.c.} \tag{A9}$$

Inserting these results into Eq. (A3) and after some rearrangements we have the field equation of motion,

$$\dot{\rho}_{nn} = -g\sum_k\{(i\sqrt{n+1}e^{-i\Omega t}\sum_{i=1}^{N}\rho_{b_i n+1,an}^k - i\sqrt{n}e^{-i\Omega t}\sum_{i=1}^{N}\rho_{b_i n,an-1}^k) + \text{c.c.}\} + \mathcal{L}_f[\rho_f]_{nn}. \tag{A10}$$

We use $\rho_f \equiv \rho$ hereafter for simplicity. Here

$$\begin{aligned}\mathcal{L}_f[\rho]_{nn} &= \langle n|\frac{\kappa}{2}(2\hat{a}\rho\hat{a}^\dagger - \rho\hat{a}^\dagger\hat{a} - \hat{a}^\dagger\hat{a}\rho)|n\rangle \\ &= \kappa\{(n+1)\rho_{n+1,n+1} - n\rho_{nn}\}.\end{aligned} \tag{A11}$$

In order to proceed with the calculation, any single term in the summation of Eq. (A10) should be calculated and inserted therein. The terms can be obtained by the integration of corresponding equation of motions by using the selecetive rules of the Hamiltonian as expressed above. We evaluate the

atomic equation of motion at zeroth order in g first, and we have

$$\dot{\rho}_A = -\frac{i}{\hbar}[H_A,\rho_A] + \gamma_{\alpha,\alpha'}\sum_{\alpha,\alpha'}\mathcal{L}[L_{\alpha,\alpha'}] + \frac{\gamma_\phi}{2}\sum_i \mathcal{L}[L_{b_i,b_i}], \tag{A12}$$

where $L_{\alpha,\alpha'} = |\alpha\rangle\langle\alpha'|$ and $L_{b_i,b_i} = |b_i\rangle\langle b_i|$. The final two terms of Eq. (A12) correspond to $\mathcal{L}_A[\rho_A]$ with $\alpha' \neq \alpha$ and $i = 1,\ldots,N$. Here $\alpha = \{a,b_1,\ldots,b_N\}$ and $\gamma_{\alpha,\alpha'}$ is taken equal to γ for simplicity. Note that the atomic part of the master equation is for the case of pure dephasing and relaxation and we follow the usual assumption of micromaser theory [24] that cavity decay and atomic dynamics can be separately treated. When the atom is inside the cavity, decay is not included.

The equation of motion of the i^{th} term of the first summation of Eq. (A10) for a single atom is

$$\dot{\rho}_{b_i n+1,an} = -ig\sqrt{n+1}e^{i\Omega t}\{\rho_{an,an} - (\rho_{b_i n+1,b_1 n+1} + \cdots + \rho_{b_i n+1,b_N n+1})\}. \tag{A13}$$

Here we have neglected the the matrix element $\langle b_i n+1|\mathcal{L}_f[\rho]|an\rangle$ in accordance with the assumptions indicated above. The equation of motion for $\rho_{b_i n,an-1}$ which is the i^{th} term of second summation of (A10) could be obtained by simply replacing $n \to n-1$ in Eq. (A13), that is,

$$\dot{\rho}_{b_i n,an-1} = -ig\sqrt{n}e^{i\Omega t}\{\rho_{an-1,an-1} - (\rho_{b_i n,b_1 n} + \cdots + \rho_{b_i n,b_N n})\}. \tag{A14}$$

Therefore we obtain the $\rho_{b_i n+1,an}$ and $\rho_{b_i n,an-1}$ terms by integrating Eqs. (A13) and (A14) formally in the following forms:

$$\rho^k_{b_i n+1,an} = -ig\sqrt{n+1}\int_{t_{k_0}}^{t} dt' e^{(i\omega_{ab_i}-\gamma)(t-t')}e^{i\Omega t'}\left\{\rho^k_{an,an} - \left(\rho^k_{b_i n+1,b_1 n+1} + \cdots + \rho^k_{b_i n+1,b_N n+1}\right)\right\}, \tag{A15}$$

$$\rho^k_{b_i n,an-1} = -ig\sqrt{n}\int_{t_{k_0}}^{t} dt' e^{(i\omega_{ab_i}-\gamma)(t-t')}e^{i\Omega t'}\left\{\rho^k_{an-1,an-1} - \left(\rho^k_{b_i n,b_1 n} + \cdots + \rho^k_{b_i n,b_N n}\right)\right\}. \tag{A16}$$

The terms of Eqs. (A15) and (A16) can be factorized to atomic and field density matrices for the zeroth-order solution in g. For instance,

$$\rho^{k_0}_{\alpha n,\alpha n}(t',t_{k_0}) = \rho^{k_0}_{\alpha,\alpha}(t',t_{k_0})\rho_{n,n}(t'), \quad \rho^{k_0}_{\alpha n+1,\alpha n+1}(t',t_{k_0}) = \rho^{k_0}_{\alpha,\alpha}(t',t_{k_0})\rho_{n+1,n+1}(t'), \tag{A17}$$

$$\rho^{k_0}_{b_i n,b_j n}(t',t_{k_0}) = \rho^{k_0}_{b_i,b_j}(t',t_{k_0})\rho_{n,n}(t'), \quad \rho^{k_0}_{b_i n+1,b_j n+1}(t',t_{k_0}) = \rho^{k_0}_{b_i,b_j}(t',t_{k_0})\rho_{n+1,n+1}(t'). \tag{A18}$$

Here $\rho^{k_0}_{\alpha,\alpha}$ and $\rho^{k_0}_{b_i,b_j}$, which are the initial atomic density matrix elements, obey the respective atomic equations of motion,

$$\dot{\rho}^{k_0}_{\alpha,\alpha}(t',t_{k_0}) = -\gamma\rho^{k_0}_{\alpha,\alpha}(t',t_{k_0}), \quad \dot{\rho}^{k_0}_{b_i,b_j}(t',t_{k_0}) = -(i\omega_{b_i b_j} + \gamma + \gamma_\phi)\rho^{k_0}_{b_i b_j}(t',t_{k_0}), \tag{A19}$$

in which the solutions are

$$\rho^{k_0}_{\alpha,\alpha} = e^{-\gamma(t-t_{k_0})}\rho^{k_0}_{\alpha,\alpha}(t_{k_0},t_{k_0}), \quad \rho^{k_0}_{b_i,b_j} = e^{-(i\omega_{b_i b_j}+\bar{\gamma})(t-t_{k_0})}\rho^{k_0}_{b_i,b_j}(t_{k_0},t_{k_0}), \tag{A20}$$

where $\bar{\gamma} = \gamma + \gamma_\phi$. Equations (A19) and (A20) imply that excited- and ground-state levels decay to a lower level. The off-diagonal elements of the atomic density matrix are equal to $\rho^{k_0}_{b_i,b_j}(t_{k_0},t_{k_0}) = |\rho^0_{b_i,b_j}|e^{i\phi_{ij}}$. The $e^{i\phi_{ij}}$ is assigned with the coherence preparation. Thus, we can express Equations (A15) and (A16) by using zeroth-order atomic Equations (A18)–(A20) to find first order solutions in g,

$$\begin{aligned}\rho^k_{b_i n+1,an} = -ig\sqrt{n+1}\int_{t_{k_0}}^{t} dt' e^{(i\omega_{ab_i}-\gamma)(t-t')}e^{i\Omega t'}\{&e^{-\gamma(t'-t_{k_0})}\rho_{aa}\rho_{nn} - e^{-\gamma(t'-t_{k_0})}\rho_{b_i b_i}\rho_{n+1n+1} \\ &- \sum_{i\neq j} e^{-(i\omega_{b_i b_j}+\bar{\gamma})(t-t_{k_0})}|\rho^0_{b_i,b_j}|e^{i\phi_{ij}}\rho_{n+1n+1}\}.\end{aligned} \tag{A21}$$

Likewise,

$$\begin{aligned}\rho^k_{b_i n,an-1} = -ig\sqrt{n}\int_{t_{k_0}}^{t} dt' e^{(i\omega_{ab_i}-\gamma)(t-t')}e^{i\Omega t'}\{&e^{-\gamma(t'-t_{k_0})}\rho^0_{aa}\rho_{n-1n-1} - e^{-\gamma(t'-t_{k_0})}\rho^0_{b_i b_i}\rho_{nn} \\ &- \sum_{i\neq j} e^{-(i\omega_{b_i b_j}+\bar{\gamma})(t-t_{k_0})}|\rho^0_{b_i,b_j}|e^{i\phi_{ij}}\rho_{nn}\}.\end{aligned} \tag{A22}$$

Putting all these results into Eq. (A10), we have the field equation of motion,

$$\begin{aligned}\dot{\rho}_{nn} = & -g^2 \sum_k \int_{t_{k_0}}^{t} dt' \Bigg\{ e^{-i\Omega(t-t')} \Bigg[(n+1) \sum_{i=1}^{N} e^{(i\omega_{ab_i}-\gamma)(t-t')} \Bigg(e^{-\gamma(t'-t_{k_0})} \rho^0_{aa} \rho_{nn} - e^{-\gamma(t'-t_{k_0})} \rho^0_{b_i b_i} \rho_{n+1n+1} \\ & - \sum_{i\neq j} e^{-(i\omega_{b_i b_j})+\gamma)(t'-t_{k_0})} \left|\rho^0_{b_i,b_j}\right| e^{i\phi_{ij}} \rho_{n+1n+1} \Bigg) - n \sum_{i=1}^{N} e^{(i\omega_{ab_i}-\gamma)(t-t')} \Bigg(e^{-\gamma(t'-t_{k_0})} \rho^0_{aa} \rho_{n-1n-1} - e^{-\gamma(t'-t_{k_0})} \rho^0_{b_i b_i} \rho_{nn} \\ & - \sum_{i\neq j} e^{(i\omega_{b_i b_j}+\bar{\gamma})(t'-t_{k_0})} \left|\rho^0_{b_i,b_j}\right| e^{i\phi_{ij}} \rho_{nn} \Bigg) \Bigg] + \text{c.c.} \Bigg\}. \end{aligned} \tag{A23}$$

Before proceeding, we replace the summation over number of injected atoms by integration over injection time as $\sum_k \to r \int_{-\infty}^{t} dk_0$ where r is the injection rate. We also define $\Delta_i = \omega_{ab_i} - \Omega$ where $\omega_{ab_i} = \omega_a - \omega_{b_i}$. Then

$$\begin{aligned}\dot{\rho}_{nn} = & -rg^2 \int_{-\infty}^{t} dt_{k_0} \int_{t_{k_0}}^{t} dt' \Bigg(\Bigg\{ \sum_{i=1}^{N} e^{(i\Delta_i-\gamma)(t'-t_{k_0})} \rho^0_{aa} [(n+1)\rho_{nn} - n\rho_{n-1n-1}] \\ & - \left[\sum_{i=1}^{N} e^{(i\Delta_i-\gamma)(t-t')} e^{-\gamma(t'-t_{k_0})} \rho^0_{b_i b_i} \right] [(n+1)\rho_{n+1n+1} - n\rho_{nn}] \\ & - \Bigg(\sum_{i<j} \left[e^{(i\Delta_i-\gamma)(t-t')} e^{-(i\omega_{b_i b_j}+\bar{\gamma})(t'-t_{k_0})} \left|\rho^0_{b_i,b_j}\right| e^{i\phi_{ij}} + e^{(i\Delta_j-\gamma)(t-t')} e^{-(-i\omega_{b_i b_j}+\bar{\gamma})(t'-t_{k_0})} \left|\rho^0_{b_i,b_j}\right| e^{-i\phi_{ij}} \right] \\ & \times \ [(n+1)\rho_{n+1n+1} - n\rho_{nn}] \Bigg\} + \text{c.c.} \Bigg) + \mathcal{L}_f[\rho]_{nn}. \end{aligned} \tag{A24}$$

Note that $\rho_{b_j b_i} = e^{-(-i\omega_{b_i b_j}+\bar{\gamma})(t-t_{k_0})} |\rho^0_{b_i,b_j}| e^{-i\phi_{ij}}$ while $\rho_{b_i b_j} = e^{-(i\omega_{b_i b_j}+\bar{\gamma})(t-t_{k_0})} |\rho^0_{b_i,b_j}| e^{i\phi_{ij}}$. Evaluating the integrals in (A24) over t' and t_{k_0} after changing integration order as $\int_{-\infty}^{t} dt_{k_0} \int_{t_{k_0}}^{t} dt' = \int_{-\infty}^{t} dt' \int_{-\infty}^{t'} dt_{k_0}$ we have

$$\begin{aligned}\dot{\rho}_{nn} = & -rg^2 \Bigg(\frac{1}{\gamma} \Bigg(\sum_{i=1}^{N} \frac{1}{-i\Delta_i + \gamma} \Bigg) \rho^0_{aa} [(n+1)\rho_{nn} - n\rho_{n-1n-1}] - \Bigg\{ \frac{1}{\gamma} \Bigg(\sum_{i=1}^{N} \frac{1}{-i\Delta_i + \gamma} \Bigg) \rho^0_{b_i b_i} \\ & + \sum_{i<j} \left[\frac{1}{(-i\Delta_i + \gamma)} \frac{1}{(i\omega_{b_i b_j} + \bar{\gamma})} e^{i\phi_{ij}} + \frac{1}{(-i\Delta_j + \gamma)} \frac{1}{(-i\omega_{b_i b_j} + \bar{\gamma})} e^{-i\phi_{ij}} \right] |\rho^0_{b_i,b_j}| \Bigg\} \\ & \times \ [(n+1)\rho_{n+1n+1} - n\rho_{nn}] + \text{c.c.} \Bigg) + \mathcal{L}_f[\rho]_{nn}. \end{aligned} \tag{A25}$$

We proceed by summing each term with their respective complex conjugates, with some rearrangements, and then,

$$\begin{aligned}\dot{\rho}_{nn} = & -rg^2 \Bigg(\frac{1}{\gamma} \Bigg(\sum_{i=1}^{N} \frac{2\gamma}{\Delta_i^2 + \gamma^2} \Bigg) \rho^0_{aa} [(n+1)\rho_{nn} - n\rho_{n-1n-1}] - \left[\frac{1}{\gamma} \Bigg(\sum_{i=1}^{N} \frac{2\gamma}{\Delta_i^2 + \gamma^2} \Bigg) \rho^0_{b_i b_i} \right] \\ & + \sum_{i<j} \Bigg\{ \left[\frac{2\cos\phi_{ij}(\Delta_i \omega_{b_i b_j} + \gamma\bar{\gamma}) + 2\sin\phi_{ij}(\omega_{b_i b_j} - \Delta_i \bar{\gamma})}{(\Delta_i^2 + \gamma^2)(\omega^2_{b_i b_j} + \bar{\gamma}^2)} + \frac{2\cos\phi_{ij}(\gamma\bar{\gamma} - \Delta_j \omega_{b_i b_j}) + 2\sin\phi_{ij}(\omega_{b_i b_j} + \Delta_j \bar{\gamma})}{(\Delta_j^2 + \gamma^2)(\omega^2_{b_i b_j} + \bar{\gamma}^2)} \right] |\rho^0_{b_i b_j}| \Bigg\} \\ & \times \ [(n+1)\rho_{n+1n+1} - n\rho_{nn}] \Bigg) \end{aligned} \tag{A26}$$

and, by using Eq. (A11), finally we have

$$\dot{\rho}_{nn} = -R\{K_a\rho_{aa}[(n+1)\rho_{nn} - n\rho_{n-1n-1}] + (R_{g_0} + R_{g_c}) \times [n\rho_{nn} - (n+1)\rho_{n+1n+1}]\} + \kappa[(n+1)\rho_{n+1,n+1} - n\rho_{nn}], \quad \text{(A27)}$$

where

$$K_a = \sum_{i=1}^{N} \frac{2}{\Delta_i^2 + \gamma^2}, \quad R_{g_0} = \sum_{i=1}^{N} K_{b_i}\rho^0_{b_ib_i}, R_{g_c} = \sum_{i<j}^{S} K_{ij}^{\phi_{ij}}\left|\rho^0_{b_ib_j}\right|, \quad K_{b_i} = \frac{2}{\Delta_i^2 + \gamma^2}, \quad \text{(A28)}$$

$$K_{ij}^{\phi_{ij}} = \frac{2\cos\phi_{ij}(\Delta_i\omega_{b_ib_j} + \gamma\bar{\gamma}) + 2\sin\phi_{ij}(\omega_{b_ib_j} - \Delta_i\bar{\gamma})}{(\Delta_i^2 + \gamma^2)(\omega_{b_ib_j}^2 + \bar{\gamma}^2)} + \frac{2\cos\phi_{ij}(\gamma\bar{\gamma} - \Delta_j\omega_{b_ib_j}) + 2\sin\phi_{ij}(\omega_{b_ib_j} + \Delta_j\bar{\gamma})}{(\Delta_j^2 + \gamma^2)(\omega_{b_ib_j}^2 + \bar{\gamma}^2)}, \quad \text{(A29)}$$

where $\Delta_{i,j} = \omega_{ab_{i,j}} - \Omega$, $\omega_{ab_{i,j}} = \omega_a - \omega_{b_{i,j}}$, and $R = rg^2$. Note that R_{g_0} has N number of terms and R_{g_c} has $S = N(N-1)/2$ number of terms in the summation. Since we seek the solutions in the steady state, we obtain the steady-state photon number $\bar{n}_\phi$ by solving $\dot{\bar{n}}_\phi = 0$, where $\dot{\bar{n}} = \sum_n n\dot{\rho}_{nn}$, and we write $\dot{\bar{n}}_\phi$ by using previously obtained $\dot{\rho}_{nn}$ as

$$\begin{aligned}\dot{\bar{n}} =& -RK_a\rho_{aa}\sum_n n(n+1)\rho_{nn} + RK_a\rho_{aa}\sum_n n^2\rho_{n-1,n-1} - RR_{g_0}\sum_n n^2\rho_{nn} + RR_{g_0}\sum_n n(n+1)\rho_{n+1,n+1} \\ & - RR_{g_c}\sum_n n^2\rho_{nn} + RR_{g_c}\sum_n n(n+1)\rho_{n+1,n+1} + \kappa\sum_n n(n+1)\rho_{n+1,n+1} - \kappa\sum_n n^2\rho_{nn}. \end{aligned} \quad \text{(A30)}$$

Then we insert $n \to n-1$ for ρ_{n+1n+1} and $n \to n+1$ for and ρ_{n-1n-1} so we get

$$\dot{\bar{n}} = RK_a\rho_{aa}\sum_n (n+1)\rho_{nn} - RR_{g_0}\sum_n n\rho_{nn} - RR_{g_c}\sum_n \rho_{nn} = RK_a\rho_{aa}(\bar{n_\phi} + 1) - R\bar{n_\phi}(R_{g_0} + R_{g_c}) - \kappa\bar{n}_\phi. \quad \text{(A31)}$$

Solving $\dot{\bar{n}}_\phi = 0$, we have

$$\bar{n}_\phi = \frac{K_a\rho_{aa}}{R_{g_0} + R_{g_c} + \frac{\kappa}{R} - K_a\rho_{aa}} = \frac{1}{\frac{R_{g_0}}{K_a\rho_{aa}} + \frac{R_{g_c}}{K_a\rho_{aa}} + \frac{\kappa}{RK_a\rho_{aa}} - 1}. \quad \text{(A32)}$$

We write the final form of the steady-state photon number after some rearrangements,

$$\bar{n}_\phi = \frac{\bar{n}_\kappa}{1 + \bar{n}_\kappa\frac{R_{g_c}}{K_a\rho_{aa}}}, \quad \text{(A33)}$$

where

$$\bar{n}_\kappa = \frac{\bar{n}}{1 + \bar{n}\frac{\kappa}{RK_a\rho_{aa}}}. \quad \text{(A34)}$$

Here $\bar{n}_\kappa$ is the average photon number in the absence of atomic coherence in terms of the average photon number $\bar{n} = 1/(R_{g_0}/K_a\rho_{aa} - 1)$, which is the average photon number in the absence of atomic coherence and in the absence of cavity decay κ.

Finally, we look at the degenerate ground-state case ($\omega_{ab_{i,j}} = 0, \Delta_{i,j} = 0$). In this case, $\bar{n}$ can be simplified to $\bar{n} = P_e/(Pg - Pe)$, where $P_e = \rho_{aa}, P_g = \rho_{b_ib_i}$ for any i. The simplified forms of other parameters are

$$K_a = \frac{2N}{\gamma^2}, \quad R_{g_0} = \frac{2NP_g}{\gamma^2}, \quad Rg_c = \frac{2N(N-1)\cos\phi\lambda}{\gamma\bar{\gamma}} \quad \text{(A35)}$$

for $\theta = \pi$. The analytical decoherence term for a degenerate case can be identified in the R_{g_c} expression such that

$$\xi = \left(1 + \frac{\gamma_\phi}{\gamma}\right)^{-1} \cong e^{-\gamma_\phi/\gamma} \quad \text{(A36)}$$

for $\gamma_\phi \ll \gamma$.

[1] S. G. Chalk and J. F. Miller, J. Power Sources **159**, 73 (2006).

[2] K. T. Chau, Y. S. Wong, and C. C. Chan, Energy Convers. Manag. **40**, 1021 (1999).

[3] Y. Yang, M. T. McDowell, A. Jackson, J. J. Cha, S. S. Hong, and Y. Cui, Nano Lett. **10**, 1486 (2010).

[4] M. O. Scully, M. S. Zubairy, G. S. Agarwal, and H. Walther, Science **299**, 862 (2003).

[5] M. O. Scully, in *AIP Conference Proceedings*, Vol. 643 (AIP, Washington DC, 2002), pp. 83–91.

[6] Y. V. Rostovtsev, Z. E. Sariyianni, and M. O. Scully, Laser Phys. **13**, 375 (2003).

[7] M. S. Zubairy, in *AIP Conference Proceedings*, Vol. 643 (AIP, Washington DC, 2002), pp. 92–97.
[8] T. D. Kieu, Phys. Rev. Lett. **93**, 140403 (2004).
[9] H. T. Quan, Y.-x. Liu, C. P. Sun, and F. Nori, Phys. Rev. E **76**, 031105 (2007).
[10] A. E. Allahverdyan, R. S. Johal, and G. Mahler, Phys. Rev. E **77**, 041118 (2008).
[11] R. S. Johal, Phys. Rev. E **80**, 041119 (2009).
[12] J. Wang, J. He, and Z. Wu, Phys. Rev. E **85**, 031145 (2012).
[13] K. E. Dorfman, D. V. Voronine, S. Mukamel, and M. O. Scully, Proc. Natl. Acad. Sci. USA **110**, 2746 (2013).
[14] H. Li, J. Zou, W.-L. Yu, L. Li, B.-M. Xu, and B. Shao, Eur. Phys. J. D **67**, 134 (2013).
[15] Z. Zhuang and S.-D. Liang, Phys. Rev. E **90**, 052117 (2014).
[16] F. Altıntaş, A. Ü. C. Hardal, and Ö. E. Müstecaplıoğlu, Phys. Rev. E **90**, 032102 (2014).
[17] F. Altıntaş, A. Ü. C. Hardal, and Ö. E. Müstecaplıoğlu, Phys. Rev. A **91**, 023816 (2015).
[18] R. Uzdin, A. Levy, and R. Kosloff, Phys. Rev. X **5**, 031044 (2015).
[19] W. Niedenzu, D. Gelbwaser-Klimovsky, A. G. Kofman, and G. Kurizki, arXiv:1508.06519v1 [quant-ph].
[20] A. Ü. C. Hardal and Ö. E. Müstecaplıoğlu, Sci. Rep. **5**, 12953 (2015).
[21] H. T. Quan, P. Zhang, and C. P. Sun, Phys. Rev. E **73**, 036122 (2006).
[22] F. Vewinger, M. Heinz, U. Schneider, C. Barthel, and K. Bergmann, Phys. Rev. A **75**, 043407 (2007).
[23] F. C. Binder, S. Vinjanampathy, K. Modi, and J. Goold, New J. Phys. **17**, 075015 (2015).
[24] P. Filipowicz, J. Javanainen, and P. Meystre, Phys. Rev. A **34**, 3077 (1986).
[25] M. Amniat-Talab, M. Saadati-Niari, S. Guérin, and R. Nader-Ali, Phys. Rev. A **83**, 013817 (2011).
[26] G. Bevilacqua, G. Schaller, T. Brandes, and F. Renzoni, Phys. Rev. A **88**, 013404 (2013).
[27] M. Saadati-Niari and M. Amniat-Talab, J. Mod. Opt. **61**, 1492 (2014).
[28] P. A. Ivanov, E. S. Kyoseva, and N. V. Vitanov, Phys. Rev. A **74**, 022323 (2006).
[29] P. A. Ivanov, B. T. Torosov, and N. V. Vitanov, Phys. Rev. A **75**, 012323 (2007).
[30] K. M. Birnbaum, A. Boca, R. Miller, A. D. Boozer, T. E. Northup, and H. J. Kimble, Nature **436**, 87 (2005).
[31] K. J. Arnold, M. P. Baden, and M. D. Barrett, Phys. Rev. A **84**, 033843 (2011).
[32] V. A. Reshetov and I. V. Yevseyev, Laser Phys. Lett. **1**, 124 (2004).
[33] E. S. Kyoseva and N. V. Vitanov, Phys. Rev. A **73**, 023420 (2006).
[34] D. D. Yavuz, J. Opt. Soc. Am. B **31**, 2665 (2014).
[35] C. Hermann-Avigliano, R. C. Teixeira, T. L. Nguyen, T. Cantat-Moltrecht, G. Nogues, I. Dotsenko, S. Gleyzes, J. M. Raimond, S. Haroche, and M. Brune, Phys. Rev. A **90**, 040502 (2014).
[36] L. Mandel and E. Wolf, *Optical Coherence and Quantum Optics*, 1st ed. (Cambridge University Press, Cambridge, 1995).
[37] J. M. Raimond, M. Brune, and S. Haroche, Rev. Mod. Phys. **73**, 565 (2001).
[38] J. R. Johansson, P. D. Nation, and F. Nori, Comput. Phys. Commun. **183**, 1760 (2012).
[39] C. Gardiner and P. Zoller, *Quantum Noise: A Handbook of Markovian and Non-Markovian Quantum Stochastic Methods with Applications to Quantum Optics*, 3rd ed. (Springer, Berlin 2010).
[40] A. Nunnenkamp, J. Koch, and S. M. Girvin, New J. Phys. **13**, 095008 (2011).
[41] H. Jirari and W. Pötz, Phys. Rev. A **72**, 013409 (2005).
[42] S. G. Schirmer and A. I. Solomon, Phys. Rev. A **70**, 022107 (2004).
[43] J. Li, M. A. Sillanpää, G. S. Paraoanu, and P. J. Hakonen, J. Phys.: Conf. Ser. **400**, 042039 (2012).
[44] N. Lu and J. A. Bergou, Phys. Rev. A **40**, 237 (1989).